






Article

Use of Photocatalytically Active Supramolecular Organic–Inorganic Magnetic Composites as Efficient Route to Remove β -Lactam Antibiotics from Water

Sabina G. Ion ^{1,2}, Octavian D. Pavel ^{1,2} , Nicolae Guzo ^{1,2}, Madalina Tudorache ^{1,2} , Simona M. Coman ^{1,2} , Vasile I. Parvulescu ^{1,2,*}, Bogdan Cojocaru ^{1,2,*}  and Elisabeth E. Jacobsen ^{3,*} 

¹ Faculty of Chemistry, University of Bucharest, 4-12 Regina Elisabeta Av., 030018 Bucharest, Romania

² Research Center for Catalysts & Catalytic Processes, Faculty of Chemistry, University of Bucharest, 4-12, Blv. Regina Elisabeta, 030018 Bucharest, Romania

³ Department of Chemistry, Norwegian University of Science and Technology, Høgskoleringen 5, 7491 Trondheim, Norway

* Correspondence: vasile.parvulescu@chimie.unibuc.ro (V.I.P.); bogdan.cojocaru@chimie.unibuc.ro (B.C.); elisabeth.e.jacobsen@ntnu.no (E.E.J.); Tel.: +40-213051464 (V.I.P. & B.C.); +47-98843559 (E.E.J.)

Abstract: Considerable efforts have been made in recent years to identify an optimal treatment method for the removal of antibiotics from wastewaters. A series of supramolecular organic-inorganic magnetic composites containing Zn-modified MgAl LDHs and Cu-phthalocyanine as photosensitizers were prepared with the aim of removing β -lactam antibiotics from aqueous solutions. The characterization of these materials confirmed the anchorage of Cu-phthalocyanine onto the edges of the LDH lamellae, with a negligible part inserted in the interlayer space. The removal of the β -lactam antibiotics occurred via concerted adsorption and photocatalytic degradation. The efficiency of the composites depended on (i) the LDH: magnetic nanoparticle (MP) ratio, which was strongly correlated with the textural properties of the catalysts, and (ii) the phthalocyanine loading in the final composite. The maximum efficiency was achieved with a removal of ~93% of the antibiotics after 2 h of reaction.

Keywords: layered double hydroxides; magnetic nanoparticles; phthalocyanines; antibiotics removal



Citation: Ion, S.G.; Pavel, O.D.; Guzo, N.; Tudorache, M.; Coman, S.M.; Parvulescu, V.I.; Cojocaru, B.; Jacobsen, E.E. Use of Photocatalytically Active Supramolecular Organic–Inorganic Magnetic Composites as Efficient Route to Remove β -Lactam Antibiotics from Water. *Catalysts* **2022**, *12*, 1044. <https://doi.org/10.3390/catal12091044>

Academic Editor: Didier Robert

Received: 15 August 2022

Accepted: 12 September 2022

Published: 14 September 2022

Publisher's Note: MDPI stays neutral with regard to jurisdictional claims in published maps and institutional affiliations.



Copyright: © 2022 by the authors. Licensee MDPI, Basel, Switzerland. This article is an open access article distributed under the terms and conditions of the Creative Commons Attribution (CC BY) license (<https://creativecommons.org/licenses/by/4.0/>).

1. Introduction

Antibiotics are by far the most successful class of drugs used to fight against bacterial infections and, therefore, they are extensively used in both the human and veterinary medicine. They are produced by both microorganisms and synthetic or semi-synthetic routes, where, regardless of the pathway, the building of the complex chemical structures generates pollutant residues [1]. Furthermore, their excretion after their use and the disposal of unused medicinal compounds are additional sources of pollution. Some antibiotics, such as penicillin, can be easily degraded, while others, such as fluoroquinolones or tetracyclines, are considerably more persistent. Accordingly, these predominate for a longer time in the environment and accumulate in higher concentrations [1]. Thus, their potential role in promoting the development of a high level of resistance to human and animal pathogens enhances the concern about their presence in the environment.

Considerable efforts have been made in recent years to identify an optimal treatment method for the removal of antibiotics from wastewaters. With this aim, advanced oxidation processes (AOP) emerged as a more promising tool compared to traditional routes, such as adsorption on activated carbon, air stripping, or reverse osmosis [2]. Indeed, many of these techniques only transfer pollutants from one phase to another, without complete destruction up to mineralization. Biological treatment is not toxic to organic cultures, but it has some limitations [3]. The most important is related to its applicability to wastewaters containing biodegradable compounds.

Among the various advanced oxidation processes, photocatalysis has emerged as a promising technology for wastewater treatment in general, and antibiotic removal in particular [4–6]. The main advantages of the process are the possibility of the simultaneous removal of antibiotics and antibiotic-resistant bacteria, the lack of mass-transfer limitations under operational environmental conditions, and the price, the commercial availability, the non-toxicity and the photochemical stability of the catalyst [7].

Recent research focused on organic photocatalysts mimicking natural supramolecular systems, in which the triplet states of the excited organic molecule can participate in electron-transfer processes in a manner that is quite similar to semiconductors [8,9]. Metallophthalocyanines (Pcs) can act as electron donors upon a photochemical excitation in the visible region [10–12]. However, the use of bare (metallo)phthalocyanines is limited due to the recovery and stability problems [13]. Therefore, their immobilization represents a viable alternative through which to solve this. TiO₂ immobilized phthalocyanines [14] or mechanical mixtures of metallophthalocyanines and zeolites [13] have already been found to be effective for the photocatalytic degradation of organic compounds. The encapsulation of these complexes in porous supports led to an increase in activity compared with the free complex, as a result of two factors: (i) the concentration of substrates around the active sites, and (ii) protection against degradation [15].

The encapsulation of metallo-phthalocyanines inside layered double hydroxides (LDHs) is another suggested solution to create hybrid organic–inorganic supramolecular systems [16]. In complement to their adsorptive and oxidation catalytic properties, LDHs were utilized in photocatalysis under both UV and Vis light irradiation [17,18]. These studies demonstrated that the immobilization of macrocyclic complexes may enhance their catalytic behavior for environmental pollution control under Vis irradiation, as well as the use of anionic phthalocyanines (sulfonated phthalocyanines) as charge-neutralizing anions [16,19–24]. However, conventional catalyst-separation methods, such as filtration or centrifugation, are not always suitable for nanoparticles due to the incomplete separation they produce. To solve this practical problem, magnetic nanoparticles (MNPs) were considered as alternative catalytic supports due to their properties, such as high surface areas and chemical stability, non-swelling properties in organic solvents [25], easy recovery by an external magnet, reusability [26], regular shapes, uniform size, low cost of production, non-toxicity, and biocompatibility [27].

β -Lactam antibiotics, such as amoxicillin (AMO), ampicillin (AMP), penicillin G (PEG), penicillin V (PEV), and cloxacillin (CLX), have antimicrobial properties through the presence of a β -lactam ring. These drugs are widely used in medicinal treatments and a high content of their metabolites ends in waste waters, which leads to several negative effects. Therefore, their removal from the environment is imperative, and various procedures involving UV irradiation [28], radiolysis [29], ozonolysis [30], Fenton- and photo-Fenton processes [28,31], photocatalysis with semiconductors [7,32–35], or a combination of these [36] have already been reported. Among these, techniques involving solar light as a source of irradiation in the photodegradation of β -lactam antibiotics are the most appropriate.

In this respect, it was already reported that AMO, AMP, PEV, PEG, or CLX can be degraded under visible irradiation by ZnS nanoparticles as photocatalysts. In a large domain of concentrations (0.5–1000 mg L⁻¹), the rate of degradation increased as the stability of the antibiotic molecules decreased [37]. ZnO nanoparticles and ZnO/polyaniline core-shell nanocomposite also degraded ampicillin under sunlight irradiation [38], while photocatalytic membranes composed of hybrid polylactic acid (PLA)/TiO₂ nanofibers deposited on fiberglass supports exhibited a high rate of degradation of AMP, which was virtually eliminated in the first 30 min of the process. Furthermore, metallic nanoparticles (Ag-NPs) were used in the photocatalytic degradation of AMP under natural sunlight irradiation with an efficiency of 96.5% [39].

However, to the best of our knowledge, MPC-LDH-MNP organic–inorganic supramolecular hybrid systems have not yet been investigated as photocatalysts for the removal of β -lactam antibiotics. Therefore, this study reports the preparation of such materials, along

with their characterization and catalytic behavior, for the photodegradation of β -lactam antibiotics under visible light. Each component in the system contributes to the photocatalysts' efficiency in the removal of antibiotics: LDH serves as a support for Pc, and is also responsible for the adsorption of the antibiotics from the environment; Pc serves as photosensitizer, and the MNPs make possible the rapid extraction of the composite from the reaction environment.

2. Results and Discussion

The coding of the catalysts based on their preparation conditions is presented in Table 1.

Table 1. The preparation details for the catalysts prepared using different LDH:MNP ratios and from different MNP precursors.

Sample	Precursor	Conditions
P1	FeCl ₂ + Fe(NO ₃) ₃	LDH:Fe ₃ O ₄ = 1:3 (10 min ageing)
P2	FeCl ₂ + Fe(NO ₃) ₃	LDH:Fe ₃ O ₄ = 1:3 (30 min ageing)
P3	FeCl ₂ + Fe(NO ₃) ₃	LDH:Fe ₃ O ₄ = 3:1 (60 min ageing)
P4	FeCl ₂ + Fe(NO ₃) ₃	LDH:Fe ₃ O ₄ = 3:2 (60 min ageing)
P5	FeCl ₂ + Fe(NO ₃) ₃	LDH:Fe ₃ O ₄ = 1:1 (60 min ageing)
P6	FeCl ₂ + Fe(NO ₃) ₃	LDH:Fe ₃ O ₄ = 1:2 (60 min ageing)
P7	FeSO ₄ + FeCl ₃ (2:1 mol)	LDH:Fe ₃ O ₄ = 3:1 (60 min ageing)
P8	FeSO ₄ + FeCl ₃ (1:2 mol)	LDH:Fe ₃ O ₄ = 3:1 (60 min ageing)

2.1. Characterization

2.1.1. X-ray Diffraction (XRD)

As previously reported [40], the X-ray diffractogram of the bare LDH shows (Figure 1a), at low angles, narrow and intense diffraction lines and, at high diffraction angles, wide and less intense lines characteristic of the LDH materials [41]. In addition to these lines, additional lines corresponding to the zincite phase (ZnO) appeared, as minor impurities, in the 2 theta range 31–38° [40]. The reconstruction by memory effect occurred with the preservation of the lines of the stable ZnO phase (ICDD 005-0664).

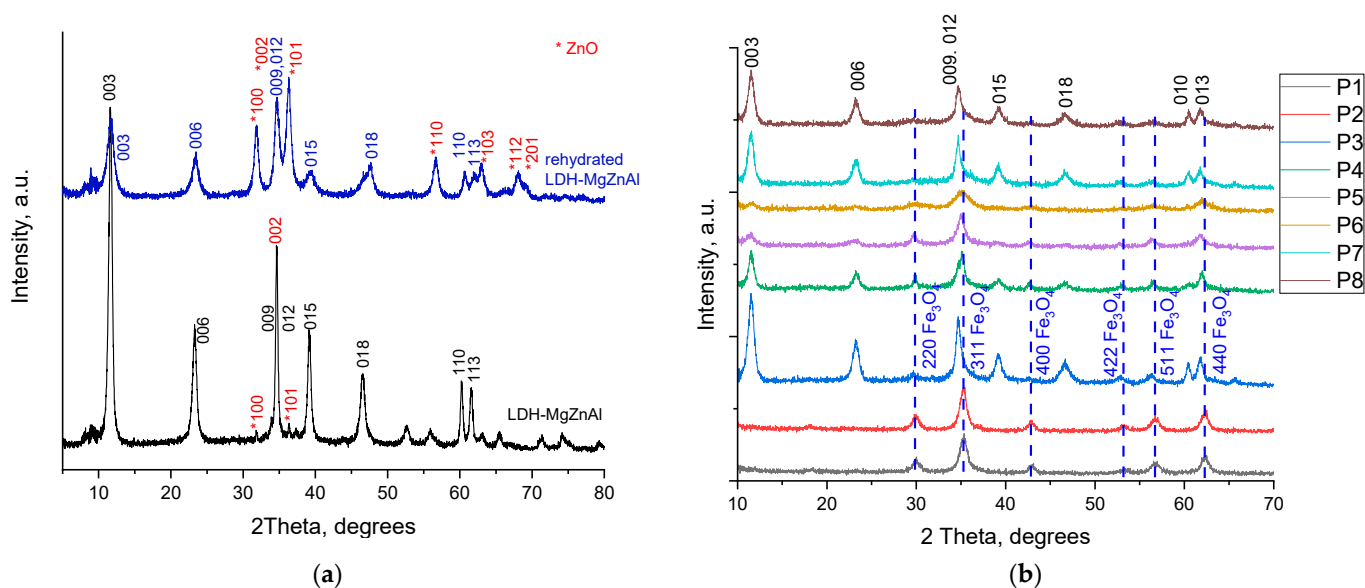


Figure 1. X-ray diffractograms corresponding to (a) as-prepared and rehydrated LDH after deposition of CuPc and (b) P1–P8 catalysts.

The X-ray diffractograms corresponding to P1–P8 catalysts are presented in Figure 1b. The magnetite phase was observed in almost all the samples and was most predominant

for P1, P2, P5, and P6. Apart from LDH, Fe₃O₄ (ICDD 19-0629), and small impurities of ZnO, no other phases or impurities were detected.

The network parameter “a” (Table 2), calculated as $a = 2 \cdot d_{110}$, indicating the average cation—cation distance in the layered network, showed a decrease in inter-layer space, as an effect of the hydration associated with the elimination, by calcination, of the larger carbonate anions that were larger, and the replacement of these by hydroxyl anions, which are much smaller in size. The network parameter “c”, calculated as $c = 3/2 \cdot (d_{003} + 2d_{006})$, keeps the trend of IFS variation caused by an increase in the electrostatic forces between the layers and the interlayer anions. According to the literature, the presence of heavy interlayer molecular species led to a change in the electron density of the 00l harmonics, i.e., organic anions [42], metal nanoparticles [43], or oxometalates [44]. Considering the “a” and “c” parameters, we can conclude that the majority of phthalocyanine is anchored on the edge of the hydroxide lamellae, while a smaller part is placed in the interplanar space. The crystallite size, which in this case was an average of the entire composite, depended on the LDH: MP ratio.

Table 2. Network parameters determined from the X-ray diffractograms for the bare MgZnAl LDH and P1–P8 catalysts.

Sample	a (Å)	c (Å)	IFS (Å) ¹	I ₀₀₃ /I ₀₀₆	I ₀₀₃ /I ₁₁₀	D(Å) ²
LDH–MgZnAl	3.0717	22.8689	2.82	2.96	5.54	132
P1	3.0462	22.5822	2.73	1.00	0.67	111
P2	3.0557	22.6262	2.74	1.08	0.68	115
P3	3.0616	22.9058	2.84	2.21	4.89	96
P4	3.0539	22.8707	2.82	2.21	6.73	105
P5	3.0644	23.1147	2.90	1.95	4.56	79
P6	3.0663	23.5299	3.04	3.00	1.29	200
P7	3.0612	22.9415	2.85	2.17	3.98	97
P8	3.0589	22.8956	2.83	2.20	4.04	95

¹ IFS represents the distance of the interplanar space (the values using Miyata’s reported sheet thickness of 4.8 Å [45]).

² The crystallite size (obtained with the Debye–Scherrer equation) and determined from the FWHM value of the reflection 003.

2.1.2. Diffuse Reflectance UV-Vis Spectroscopy (DR-UV-Vis)

The bare LDH showed a wide absorption band in the range of 240–380 nm, with maxima at 348 and 359 nm corresponding to a zincite phase in the layered structure (Figure 2a) [40]. The additional band at 212 nm corresponds to Mg(OH)₂/MgO [40,46], while those in the region 550–750 nm to the strong Q bands, assigned to the CuPc [47]. The DR-UV-Vis spectra of the phthalocyanine-LDH composites are presented in Figure 2b. These disclose B-bands of CuPc (300–350 nm) [48] and magnetite 500 nm [49].

2.1.3. Diffuse-Reflectance Infrared Spectroscopy (DRIFT)

The intercalation of phthalocyanine was also confirmed by the DRIFT analysis (Figure 3). Regarding the LDH (Figure 3a), the wide absorption band located in the 3700–3400 cm^{−1} range corresponds to the vibrations of the OH, ν(O–H) groups in the interplanar space, while the band at 3000 cm^{−1} was assigned to the hydrogen bonds between the water and the carbonate anion [50]. The band at 1638–1650 cm^{−1} corresponded to the vibrations of the water molecules in the layered structure, that in the range 1100 and 650 cm^{−1} to the vibrations of the CO₃^{2−} groups, and those before 600 cm^{−1} to the Mg–O, Zn–O and Al–O bonds. The infrared spectra also showed some bands associated with the presence of LDH-anchored phthalocyanine [51] (Figure 3b), although their intensity was very low. For example, the band at approximately 1650 cm^{−1} was assigned to the C=N bond, that at 1120 cm^{−1} to the S=O bond, and those at 730, 1033 and 1090 cm^{−1} to the C–H bond.

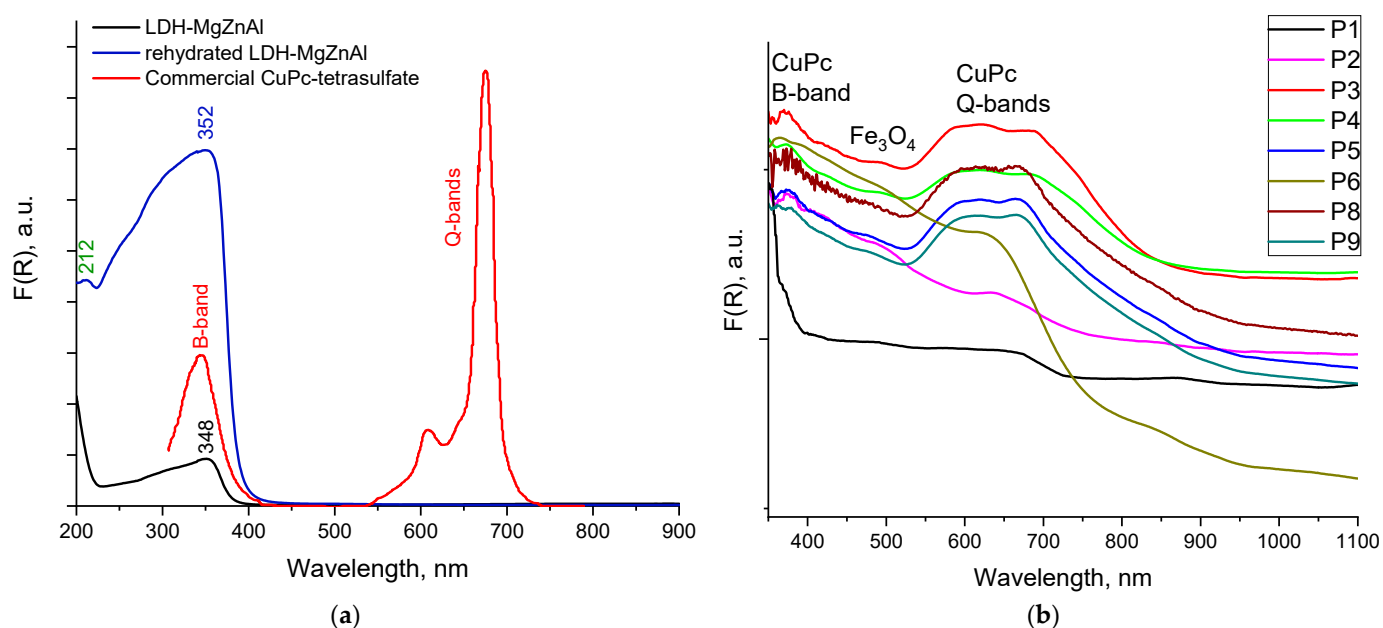


Figure 2. DR-UV-VIS spectra collected for (a) as-prepared and rehydrated LDH, commercial CuPc tetrasulfate, and (b) P1–P8 catalysts.

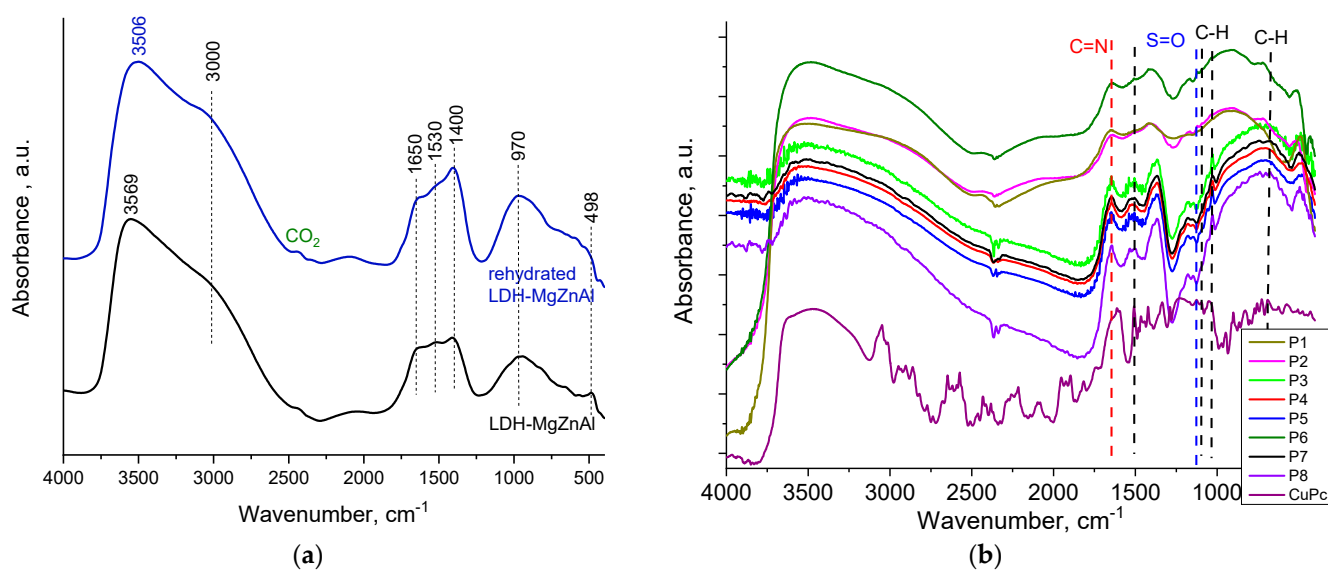


Figure 3. DRIFT spectra collected for (a) as-prepared and rehydrated LDH and (b) P1–P8 catalysts and commercial CuPc tetrasulfate.

2.1.4. Textural Properties

The surface areas of the P1–P8 catalysts (Table 2) varied in a rather narrow range, i.e., from 110 (P4) to 160 m²·g⁻¹ (P5). The increase in the ageing time, which also meant an increase in the MNP size, led to a decrease in the surface area (samples P1 and P2). The decrease of the surface area compared to the parent LDH was due to the tendency to clusterize in large conglomerates systems confirmed by TEM (see Supplementary Materials) [52]. All the samples presented a Type IV adsorption–desorption isotherm, characteristic of mesoporous materials (Figure 4). However, depending on the LDH: MNP ratio and the nature of MNP precursors, the variation in the pore size was larger (Table 3, Figure 4).

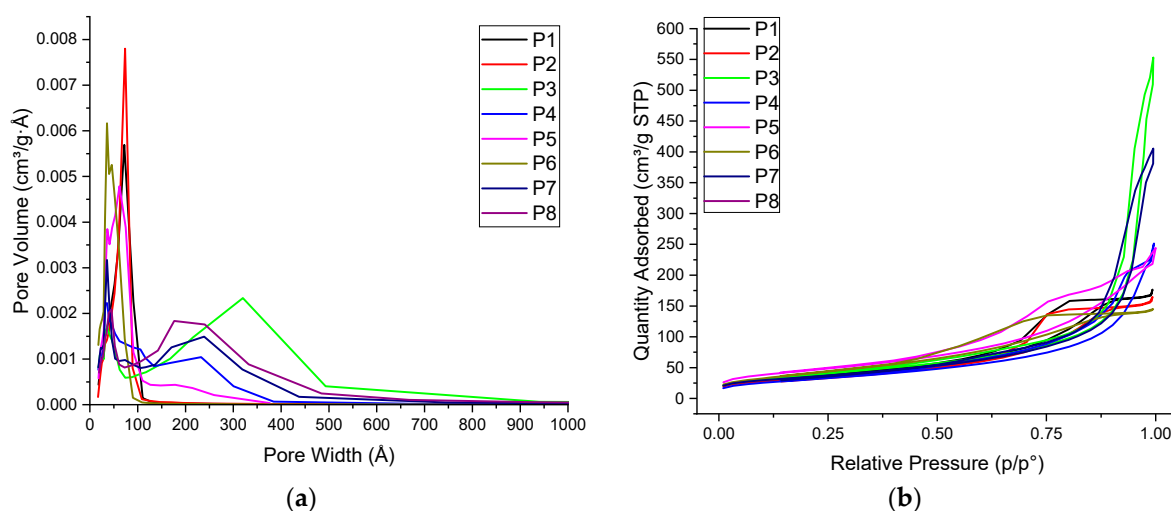


Figure 4. Pore-size distribution (a) and adsorption–desorption isotherms (b) for the P1–P8 catalysts.

Table 3. Surface area, pore volume, and main pore size for LDH, rehydrated LDH, and P1–P8 catalysts.

Sample	S_s (BET) ($\text{m}^2 \cdot \text{g}^{-1}$)	Pore Volume ($\text{cm}^3 \cdot \text{g}^{-1}$)	Average Pore Size (Å)
LDH-MgZnAl	69	0.387	222
Rehydrated LDH-MgZnAl	25	0.186	238
P1	129	0.277	72
P2	116	0.258	73
P3	137	0.858	34, 317
P4	111	0.392	34, 90, 231
P5	163	0.336	37, 63, 182
P6	148	0.230	36, 45
P7	124	0.628	~200
P8	124	0.498	~200

2.2. Degradation of Antibiotics

The experiments carried out in this study for the removal of antibiotics from water using the organic–inorganic magnetic composite photocatalysts indicated two parallel processes, namely, adsorption and photocatalytic degradation (Figures 5 and 6, respectively).

Simple adsorption measurements (i.e., in the absence of photo-irradiation) indicated a removal of ampicillin of 9–87%. Depending on the catalyst, the removal of the ampicillin varied in the following order: P7 > P3 > P8 > P5 > P6 > P4 > P2–P1, i.e., in good concordance with their textural properties (pore volume and interlayer diameter). Although P3 had the highest pore volume in the series, it presented some interlayer limitation disfavoring the adsorption of ampicillin. For mesoporous supports with larger pores (200–700 nm), the loading of the adsorbed ampicillin does not depend on the pore size, and it was related only to the surface charge density (σ) of the sorbent surface [53]. For the LDHs, the ampicillin-related amoxicillin was found to adsorb predominantly by a chemisorption mechanism, following pseudo-second-order kinetics [54]. Indeed, as shown in Table 3, the interlayer distance did not influence the mass transfer or the access to the chemisorption sites.

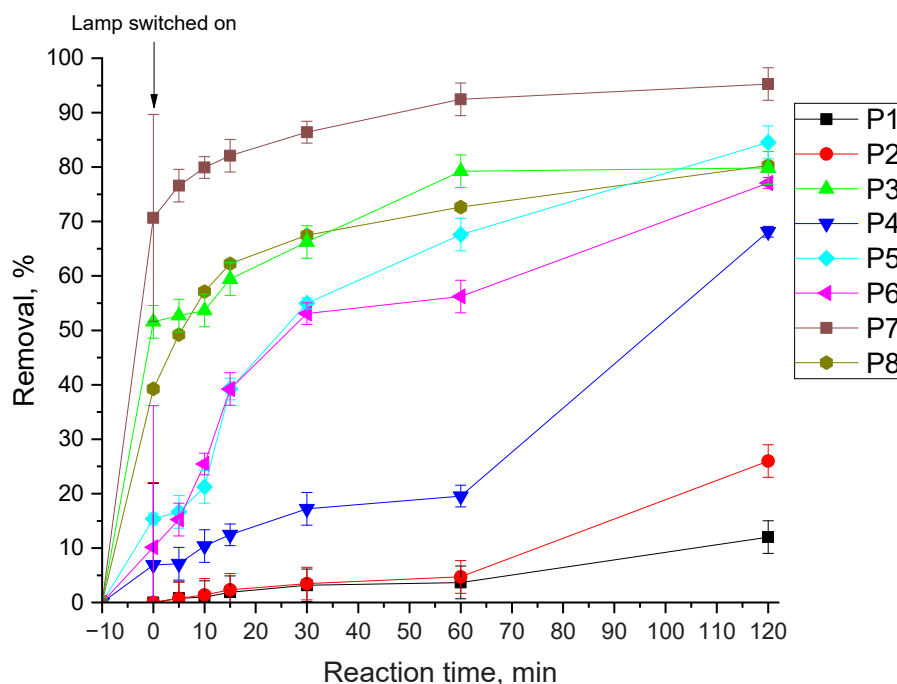


Figure 5. Removal of ampicillin from water solution using a blue LED (445–465 nm) as irradiation source.

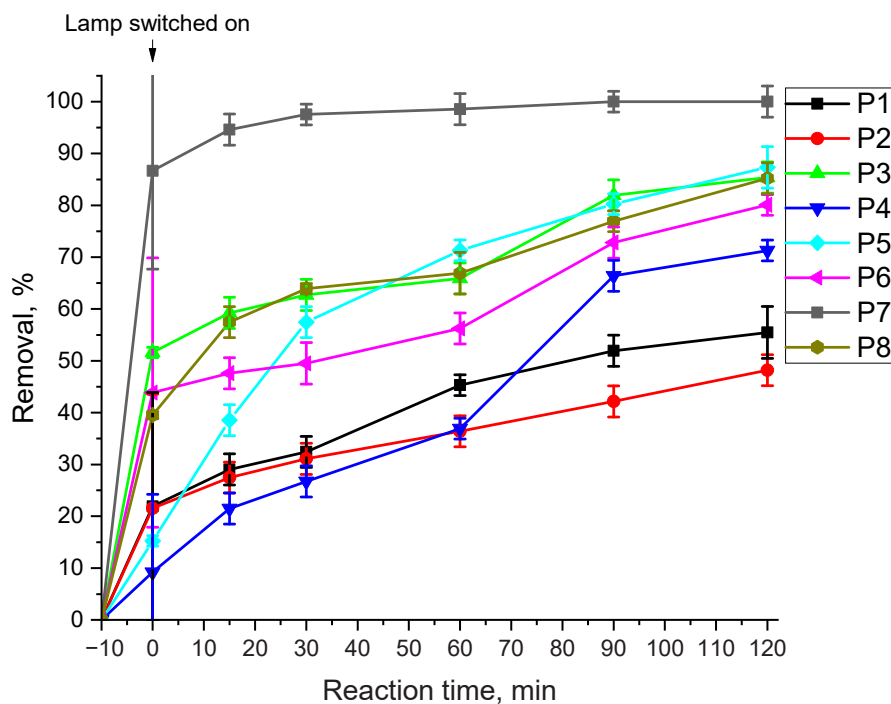


Figure 6. Removal of ampicillin from water solution using a solar simulator as irradiation source.

The photo-irradiation of the system changed the order established by the adsorption. However, the photo-catalytic degradation could not be separated from the adsorption of the ampicillin and degraded fragments, and it was also dependent on the photo-irradiation energy. Under the LED irradiation (the initial concentration of ampicillin in solution at $t = 0$), the maximum degradation was achieved for P7, with a removal of ~93% after 2 h of reaction. Overall, summarizing the effects of the adsorption and photocatalytic degradation, the removal decreased in the following order: P7 > P5 > P8~P3 > P6 > P4 > P2 > P1 (Figure 5).

The performances of these catalysts depended both on the LDH:MNP ratio (which was also associated with the amount of CuPc) and the textural properties of the composite.

Moving to a solar simulator as an irradiation source (Figure 6) afforded a higher removal efficiency, which was correlated with the higher photocatalytic efficiency attributed to the absorption of the light via the Q bands of the phthalocyanine.

The stability and reusability of catalysts are very important factors in the characterization of their efficiency and the limits of their applicability in real applications. Based on these considerations, the composite P7 demonstrated an enhanced efficiency. After three runs (the catalyst was magnetically removed from the reaction environment, washed thoroughly with deionized water, and then dried at 120 °C for 4 h) the conversion of the ampicillin was conserved at 98%. After each run, the DRIFT analysis confirmed no leaching of the phthalocyanine (Figure 7).

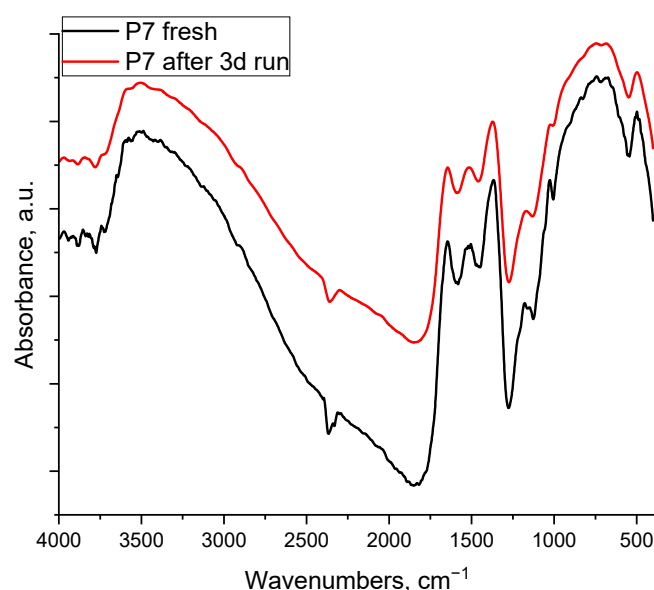


Figure 7. DRIFT spectra of fresh and spent P7 sample.

Similar tests on the removal of amoxicillin under simulated solar-light irradiation (Figure 8) using selected composites confirmed the order of activity determined for the ampicillin. However, both the absorption part and the photocatalytic behavior showed some differences. These were directly related to the structural features of these antibiotics (Figure 8), which can affect both the adsorption of molecules and photocatalytic degradation processes. Thus, the degradation of β -lactam antibiotics can follow two routes: hydroxylation and opening of the β -lactam ring [55]. The ratio between these routes is influenced by the structure of the antibiotic and the nature of the catalyst. For example, hydroxylation can be enhanced for amoxicillin compared to ampicillin by the population and the strength of the hydroxyl groups able to activate the aromatic ring, making it more susceptible to their attachment. However, the mechanism of the photo-degradation of β -lactam antibiotics is still under discussion.

FTIR analysis of the amoxicillin solution in the presence of P7 sample at each reaction time shows an increase in the amount of bonds involving oxygen (Figure 9a–c), which back up both reaction pathways.

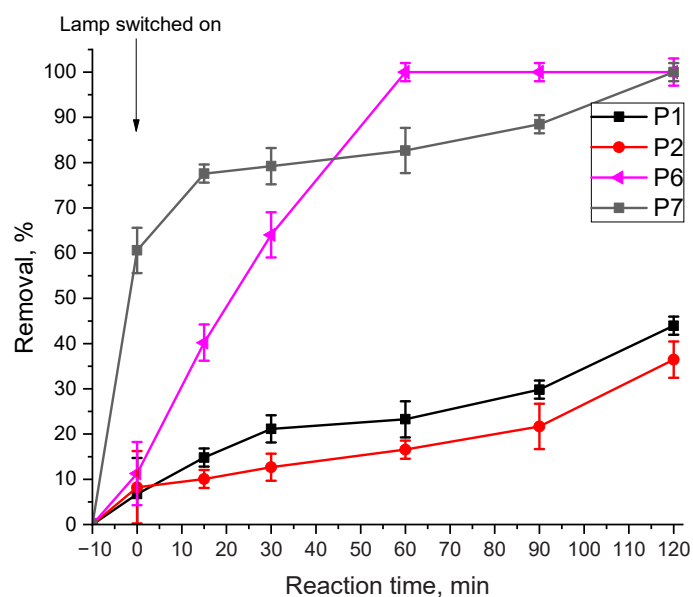


Figure 8. Example of removal of amoxicillin from water solution using a solar simulator as an irradiation source.

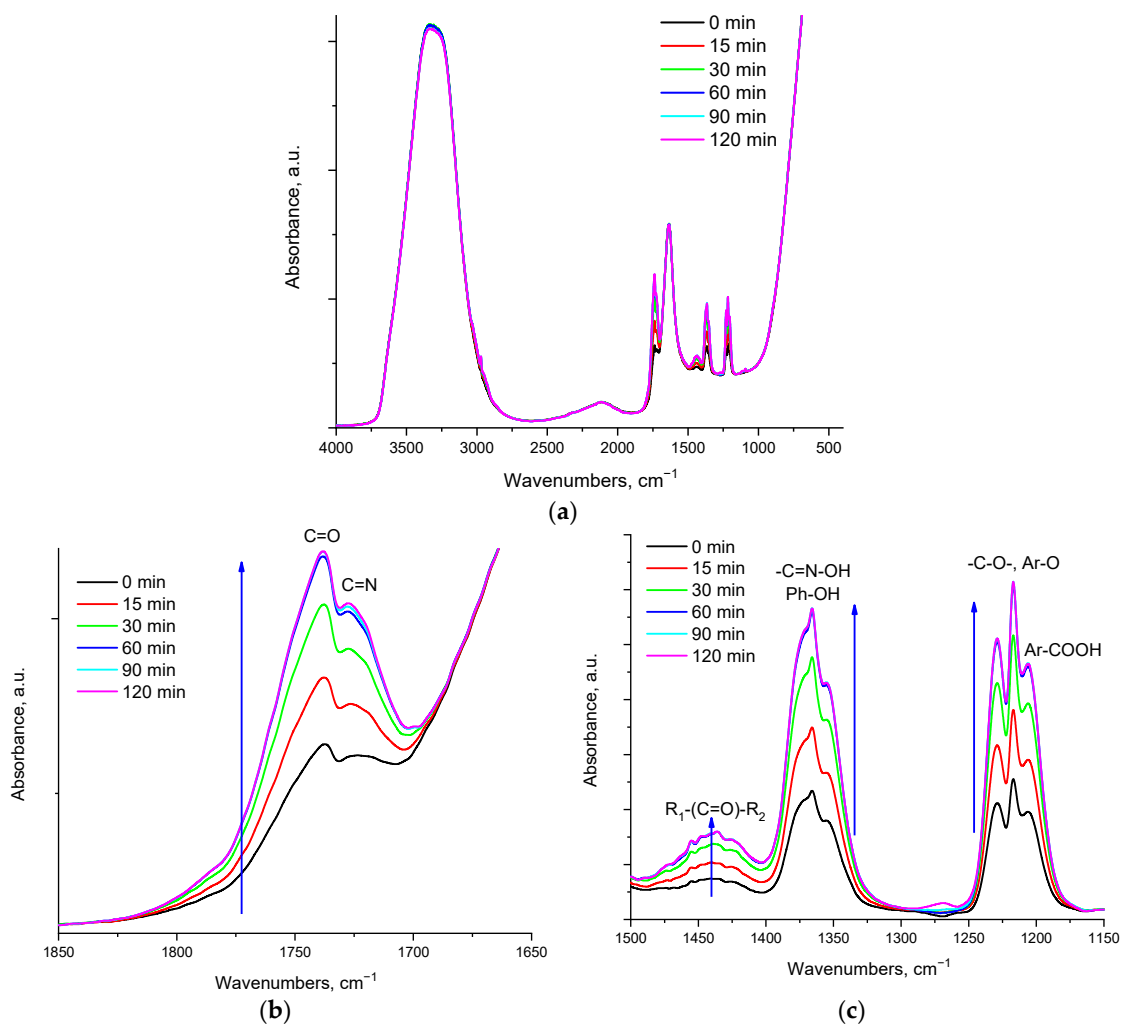


Figure 9. FTIR spectra of amoxicillin solution in the presence of P7 sample at each reaction time: (a) full spectra, (b) $1850\text{--}1650\text{ cm}^{-1}$ region, (c) $1500\text{--}1150\text{ cm}^{-1}$ region.

3. Materials and Methods

3.1. Synthesis

The synthesis of LDH $\text{Mg}_{0.375}\text{Zn}_{0.375}\text{Al}_{0.25}$ was carried out following a previously reported procedure [40]. Therefore, two solutions (A and B), were mixed at an inlet flow of $1 \text{ cm}^3 \cdot \text{min}^{-1}$, at RT under stirring (600 rpm). Solution A of a concentration of 1.5M contained the nitrate-like precursors of Mg, Zn, and Al in the molar ratio $\text{Mg}/\text{Zn}/\text{Al} = 0.375/0.375/0.25$. The base solution contained 0.23 moles NaOH and 0.092 moles Na_2CO_3 at a concentration of 1M in Na_2CO_3 . Co-precipitation of these took place for 1.5 h at the pH of 10 ± 0.2 (continuously monitored by a pH-meter, pH315i), after which the resulted precipitate was aged for 18 h, at 80°C , in air atmosphere at the same stirring rate. The suspension was then cooled at room temperature, filtered under vacuum, and washed with distilled water until reaching a pH of 7. The precipitate was dried at 120°C for 24 h in air atmosphere, resulting in LDH-MgZnAl. The insertion of phthalocyanine into the structure of LDH started from the calcination of LDH for 18 h at 460°C ($10^\circ\text{C}/\text{min}$), followed by stirring of the resulting mixed oxide with a solution of Co-phthalocyanine 3,4',4'',4'''-tetrasulfonic acid (0.1 M) for 12 h, filtration of the composite phthalocyanine-LDH, washing of the precipitate, and drying at 120°C for 24 h in air. The amount of CuPc determined by elemental analysis was $\sim 10 \times 10^{-5}$ moles CuPc/g of LDH.

The attachment of the magnetic particles (MPs) was achieved by mixing 100 mg of modified LDH with Cu-phthalocyanine in 100 mL of water. After vigorous stirring for 10 min, the corresponding amounts of FeCl_2 and $\text{Fe}(\text{NO}_3)_3$ were added, resulting in a $\text{MP@CuPc@LDH-MgZnAl}$ composite. The mixture was then heated at 70°C in an oil bath and treated, by a slow addition, with 7.5 mL of 5M NaOH. The resulting suspension was then left to age for 60 min. Finally, the solid was magnetically removed, washed with water by decantation, and dried at 70°C for 12 h.

In order to verify the structural influence of the LDH: MNPs ratio and the nature of the MNP precursors, a series of materials containing CuPc@LDH-MgZnAl were prepared using a similar protocol (Table 1).

3.2. Characterization

3.2.1. Specific Surface Area (BET) and Pore-Size Measurements

The investigation of the textural characteristics was performed using the 77K nitrogen adsorption–desorption isotherms collected using a Micromeritics ASAP2020 Surface Area and Porosity Analyzer. The samples were outgassed under vacuum for 24 h at 120°C .

3.2.2. X-ray Diffraction (XRD)

XRD data were collected at room temperature using a Shimadzu XRD-7000 apparatus taking the monochromatic $\text{Cu K}\alpha$ radiation ($\lambda = 1.5406 \text{ \AA}$, 40 kV, 40 mA), with a scanning rate of 0.1 degrees per minute, in the range $2\theta = 5\text{--}80$ degrees.

The size of the crystallites was estimated using Sherrer's equation:

$$D = k \cdot \lambda / \text{FWHM} \cdot \sin\theta \quad (1)$$

where:

$k = 0.9$ (shape factor)

λ = wavelength of the X-ray radiation source (for Cu = 1.54 \AA)

FWHM = full width at half height (in radians)

θ = maximum position (in radians)

3.2.3. Diffuse-Reflectance UV-Vis Spectroscopy (DR-UV-Vis)

The DR-UV-Vis spectra were collected under ambient conditions using Specord 250 equipment (Analytic Jena) with an integrating sphere as a measuring device in the reflectance mode. MgO was used as reference material.

3.2.4. Diffuse-Reflectance Infrared Spectroscopy (DRIFT)

The infrared spectra were collected with a Bruker Tensor II device equipped with a Harrick Praying Mantis Diffuse Reflection accessory. The final spectra averaged 128 scans with a resolution of 4 cm^{-1} . KBr was used as a reference.

3.3. Photocatalytic Tests

The irradiation was generated by a sunlight simulator using a Luzchem LZC-4b source (LED 445–465 nm), or a Sciencetech SF150-A Small Collimated Beam Solar Simulator (equipped with Air Mass AM1.5G Filter and Light-Tight Reaction Chamber). The evolution of the photocatalyzed reaction was followed by means of a liquid chromatograph (HPLC) equipped with Zorbax SB-C18 column ($4.6 \times 150\text{ mm}$, 5 microns), mobile phase 25 mM KH_2PO_4 :ACN = 60:40, mobile phase flow $0.5\text{ mL}\cdot\text{min}^{-1}$; analysis time 30 min; column temperature $60\text{ }^\circ\text{C}$, DAD detection 204 nm). In a typical experiment, 15 mL of a prepared 0.015 M solution of antibiotic and 60 mg of catalyst were added into a quartz test tube. To establish the absorption–desorption equilibrium; before turning on the lamp, the samples were kept in the dark, under stirring, for 10 min.

4. Conclusions

A series of supramolecular organic–inorganic magnetic composites containing Zn-modified MgAl-LDHs and Cu-phthalocyanine as photosensitizers were prepared with the aim of removing β -lactam antibiotics from aqueous solutions. The resulting composites were characterized using textural, spectral, and diffractometric techniques. These confirmed the anchorage of Cu-phthalocyanine onto the edges of the LDH lamellae, without any insertion in the interlayer space. The removal of these antibiotics occurred via concerted adsorption and photocatalytic degradation. The efficiency of the composites depended on (i) the LDH:MP ratio, which was strongly correlated with the textural properties of the catalysts, and (ii) the phthalocyanine loading in the final composite. The maximum efficiency was achieved for the P8 photocatalyst, with a removal of $\sim 93\%$ ampicillin after 2 h of reaction.

Supplementary Materials: The following supporting information can be downloaded at: <https://www.mdpi.com/article/10.3390/catal12091044/s1>, Figure S1: TEM image of fresh LDH; Figure S2: TEM image of rehydrated LDH; Figure S3: TEM image of MNP@ rehydrated LDH. Reference [52] is cited in the Supplementary Materials.

Author Contributions: Conceptualization, B.C.; methodology, B.C. and O.D.P.; investigation, S.G.I., N.G., O.D.P., M.T. and S.M.C.; resources, B.C. and E.E.J.; writing—original draft preparation, B.C., O.D.P. and E.E.J.; writing—review and editing, V.I.P., B.C., O.D.P. and E.E.J.; supervision, B.C. and M.T.; funding acquisition, M.T. and E.E.J. All authors have read and agreed to the published version of the manuscript.

Funding: This work was supported by a grant of The Romanian Ministry of Education and Research, CNCS-UEFISCDI, project number PN-III-P4-ID-PCE-2020-2207, within PNCDI III, and by The Education, Scholarship, Apprenticeships and Youth Entrepreneurship Programme–EEA, grants 2014–2021, project no. 18-Cop-0041.

Data Availability Statement: The data are available on request from the corresponding author.

Conflicts of Interest: The authors declare no conflict of interest.

References

1. Martinez, J.L. Environmental pollution by antibiotics and by antibiotic resistance determinants. *Environ. Pollut.* **2009**, *157*, 2893–2902. [[CrossRef](#)] [[PubMed](#)]
2. Zhang, G.; Ji, S.; Xi, B. Feasibility study of treatment of amoxicillin wastewater with a combination of extraction, Fenton oxidation and reverse osmosis. *Desalination* **2006**, *196*, 32–42. [[CrossRef](#)]
3. Surenjan, A.; Pradeep, T.; Philip, L. Application and performance evaluation of a cost-effective vis- LED based fluidized bed reactor for the treatment of emerging contaminants. *Chemosphere* **2019**, *228*, 629–639. [[CrossRef](#)] [[PubMed](#)]

4. Liu, C.; Mao, S.; Wang, H.; Wu, Y.; Wang, F.; Xia, M.; Chen, Q. Peroxymonosulfate-assisted for facilitating photocatalytic degradation performance of 2D/2D WO₃/BiOBr S-scheme heterojunction. *Chem. Eng. J.* **2022**, *430*, 132806. [[CrossRef](#)]
5. Liu, C.; Mao, S.; Shi, M.; Wang, F.; Xia, M.; Chen, Q.; Ju, X. Peroxymonosulfate activation through 2D/2D Z-scheme CoAl-LDH/BiOBr photocatalyst under visible light for ciprofloxacin degradation. *J. Hazard. Mater.* **2021**, *420*, 126613. [[CrossRef](#)] [[PubMed](#)]
6. Liu, C.; Mao, S.; Shi, M.; Hong, X.; Wang, D.; Wang, F.; Xia, M.; Chen, Q. Enhanced photocatalytic degradation performance of BiVO₄/BiOBr through combining Fermi level alteration and oxygen defect engineering. *Chem. Eng. J.* **2022**, *449*, 137757. [[CrossRef](#)]
7. Elmolla, E.S.; Chaudhuri, M. Photocatalytic degradation of amoxicillin, ampicillin and cloxacillin antibiotics in aqueous solution using UV/TiO₂ and UV/H₂O₂/TiO₂ photocatalysis. *Desalination* **2010**, *252*, 46–52. [[CrossRef](#)]
8. Bobo, M.V.; Kuchta, J.J.I.; Vannucci, A.K. Recent advancements in the development of molecular organic photocatalysts. *Org. Biomol. Chem.* **2021**, *19*, 4816–4834. [[CrossRef](#)]
9. Romero, N.A.; Nicewicz, D.A. Organic Photoredox Catalysis. *Chem. Rev.* **2016**, *116*, 10075–10166. [[CrossRef](#)]
10. Schmidt, A.M.; Calvete, M.J.F. Phthalocyanines: An Old Dog Can Still Have New (Photo)Tricks! *Molecules* **2021**, *26*, 2823. [[CrossRef](#)]
11. Vallejo Lozada, W.A.; Diaz-Urbe, C.; Quiñones, C.; Lerma, M.; Fajardo, C.; Navarro, K. Phthalocyanines: Alternative Sensitizers of TiO₂ to be Used in Photocatalysis. In *Phthalocyanines and Some Current Applications*; Yilmaz, Y., Ed.; IntechOpen: London, UK, 2017. [[CrossRef](#)]
12. Ion, R. Porphyrins and Phthalocyanines: Photosensitizers and Photocatalysts. In *Phthalocyanines and Some Current Applications*; Yilmaz, Y., Ed.; IntechOpen: London, UK, 2017. [[CrossRef](#)]
13. Corma, A.; Garcia, H. Zeolite-based photocatalysts. *Chem. Commun.* **2004**, 1443–1459. [[CrossRef](#)] [[PubMed](#)]
14. Ranjit, K.T.; Willner, I.; Bossmann, S.; Braun, A. Iron(III) phthalocyanine-modified titanium dioxide: A novel photocatalyst for the enhanced photodegradation of organic pollutants. *J. Phys. Chem. B* **1998**, *102*, 9397–9403. [[CrossRef](#)]
15. Zsigmond, A.; Notheisz, F.; Bäckvall, J.-E. Rate enhancement of oxidation reactions by the encapsulation of metal phthalocyanine complexes. *Catal. Lett.* **2000**, *65*, 135–139. [[CrossRef](#)]
16. Perez-Bemal, E.; Ruano-Casero, R.; Pinnavaia, T.J. Catalytic autoxidation of 1-decanethiol by cobalt(II) phthalocyaninetetrasulfonate intercalated in a layered double hydroxide. *Catal. Lett.* **1991**, *11*, 55. [[CrossRef](#)]
17. Mohapatra, L.; Parida, K. A review on the recent progress, challenges and perspective of layered double hydroxides as promising photocatalysts. *Mater. Chem. A* **2016**, *4*, 10744. [[CrossRef](#)]
18. Gao, L.-G.; Gao, Y.-Y.; Song, X.-L.; Ma, X.-R. A novel La³⁺-Zn²⁺-Al³⁺-MoO₄²⁻ layered double hydroxides photocatalyst for the decomposition of dibenzothiophene in diesel oil. *Pet. Sci. Technol.* **2018**, *36*, 850–855. [[CrossRef](#)]
19. Barbosa, C.A.S.; Ferrira, A.M.D.C.; Constantino, V.R.L.; Coelho, A.C.V. Preparation and Characterization of Cu(II) Phthalocyanine Tetrasulfonate Intercalated and Supported on Layered Double Hydroxides. *J. Incl. Phenom. Macro. Chem.* **2002**, *42*, 15. [[CrossRef](#)]
20. Barbosa, C.A.S.; Dias, P.M.; Ferrira, A.M.C.; Constantino, V.R.L. Mg–Al hydrotalcite-like compounds containing iron-phthalocyanine complex: Effect of aluminum substitution on the complex adsorption features and catalytic activity. *Appl. Clay Sci.* **2005**, *28*, 147. [[CrossRef](#)]
21. Barbosa, C.A.S.; Ferrira, A.M.D.C.; Constantino, V.R.L. Synthesis and Characterization of Magnesium-Aluminum Layered Double Hydroxides Containing (Tetrasulfonated porphyrin)cobalt. *Eur. J. Inorg. Chem.* **2005**, 1577. [[CrossRef](#)]
22. Kanan, S.; Awate, S.V.; Agashe, M.S. Incorporation of anionic copper phthalocyanine complexes into the intergallery of Mg-Al layered double hydroxides. *Stud. Surf. Sci. Catal.* **1998**, *113*, 927. [[CrossRef](#)]
23. Parida, K.M.; Baliarsingh, N.; Sairam Patra, B.; Das, J. Copperphthalocyanine immobilized Zn/Al LDH as photocatalyst under solar radiation for decolorization of methylene blue. *J. Mol. Catal. A Chem.* **2007**, *267*, 202–208. [[CrossRef](#)]
24. Maretti, L.; Carbonell, E.; Alvaro, M.; Scaiano, J.C.; Garcia, H. Laser flash photolysis of dioxo iron phthalocyanine intercalated in hydrotalcite and its use as a photocatalyst. *J. Photochem. Photobio. A Chem.* **2009**, *205*, 19–22. [[CrossRef](#)]
25. Abu-Reziq, R.; Alper, H.; Wang, D.; Post, M.L. Metal Supported on Dendronized Magnetic Nanoparticles: Highly Selective Hydroformylation Catalysts. *J. Am. Chem. Soc.* **2006**, *128*, 5279–5282. [[CrossRef](#)]
26. Karaoğlu, E.; Baykal, A.; Erdemi, H.; Alpsoy, L.; Sozeri, H. Synthesis and characterization of dl-thioctic acid (DLTA)–Fe₃O₄ nanocomposite. *J. Alloys Compd.* **2011**, *509*, 9218–9225. [[CrossRef](#)]
27. Naeimi, H.; Nazifi, Z.S. A highly efficient nano-Fe₃O₄ encapsulated-silica particles bearing sulfonic acid groups as a solid acid catalyst for synthesis of 1,8-dioxo-octahydroxanthene derivatives. *J. Nanopart. Res.* **2013**, *15*, 2026–2032. [[CrossRef](#)] [[PubMed](#)]
28. Brillas, E. A review on the photoelectro-Fenton process as efficient electrochemical advanced oxidation for wastewater remediation. Treatment with UV light, sunlight, and coupling with conventional and other photo-assisted advanced technologies. *Chemosphere* **2020**, *250*, 126198. [[CrossRef](#)]
29. Szabó, L.; Tóth, T.; Engelhardt, T.; Rácz, G.; Mohácsi-Farkas, S.; Takács, E.; Wojnárovits, L. Change in hydrophilicity of penicillins during advanced oxidation by radiolytically generated OH compromises the elimination of selective pressure on bacterial strains. *Sci. Total Environ.* **2016**, *551–552*, 393–403. [[CrossRef](#)]
30. Andreozzi, R.; Canterino, M.; Marotta, R.; Paxeus, N. Antibiotic removal from wastewaters: The ozonation of amoxicillin. *J. Hazard. Mater.* **2005**, *122*, 243–250. [[CrossRef](#)]

31. Rozas, O.; Contreras, D.; Mondaca, M.A.; Pérez-Moya, M.; Mansilla, H.D. Experimental design of Fenton and photo-Fenton reactions for the treatment of ampicillin solutions. *J. Haz. Mat.* **2010**, *177*, 1025–1030. [[CrossRef](#)]
32. Belhacova, L.; Bibova, H.; Marikova, T.; Kuchar, M.; Zouzelka, R.; Rathousky, J. Removal of Ampicillin by Heterogeneous Photocatalysis: Combined Experimental and DFT Study. *Nanomaterials* **2021**, *11*, 1992. [[CrossRef](#)]
33. Dimitrakopoulou, D.; Rethemiotaki, I.; Frontistis, Z.; Xekoukoulotakis, N.P.; Venieri, D.; Mantzavinos, D. Degradation, mineralization and antibiotic inactivation of AMX by UV-A/TiO₂ photocatalysis. *J. Environ. Manag.* **2012**, *98*, 168–174. [[CrossRef](#)] [[PubMed](#)]
34. Klauson, D.; Babkina, J.; Stepanova, K.; Krichevskaya, M.; Preis, S. Aqueous photocatalytic oxidation of amoxicillin. *Catal. Today* **2010**, *151*, 39–45. [[CrossRef](#)]
35. Shaykhi, Z.M.; Zinatizadeh, A.A.L. Statistical modeling of photocatalytic degradation of synthetic AMX wastewater in an immobilized TiO₂ photocatalytic reactor using response surface methodology. *J. Taiwan Inst. Chem. Eng.* **2014**, *45*, 1717–1726. [[CrossRef](#)]
36. Hou, J.; Chen, Z.; Gao, J.; Xie, Y.; Li, L.; Qin, S.; Wang, Q.; Mao, D.; Luo, Y. Simultaneous removal of antibiotics and antibiotic-resistance genes from pharmaceutical wastewater using the combinations of up-flow anaerobic sludge bed, anoxic-oxic tank, and advanced oxidation technologies. *Water Res.* **2019**, *159*, 511–520. [[CrossRef](#)] [[PubMed](#)]
37. Pouredal, H.R.; Hasanali, M.A. Photocatalytic degradation of some β -lactam antibiotics in aqueous suspension of ZnS nanoparticles. *Desalination Water Treat.* **2013**, *51*, 2617–2623. [[CrossRef](#)]
38. Nosrati, R.; Olad, A.; Maramifar, R. Degradation of ampicillin antibiotic in aqueous solution by ZnO/polyaniline nanocomposite as photocatalyst under sunlight irradiation. *Environ. Sci. Pollut. Res.* **2012**, *19*, 2291–2299. [[CrossRef](#)]
39. Jassal, P.S.; Khajuria, R.; Sharma, R.; Debnath, P.; Verma, S.; Johnson, A.; Kumar, S. Photocatalytic degradation of ampicillin using silver nanoparticles biosynthesized by *Pleurotus ostreatus*. *BioTechnologia* **2020**, *101*, 5–14. [[CrossRef](#)]
40. Zăvoianu, R.; Mihăilă, S.-D.; Cojocaru, B.; Tudorache, M.; Parvulescu, V.I.; Pavel, O.D.; Oikonomopoulos, S.; Jacobsen, E.E. An advanced approach for MgZnAl-LDH catalysts synthesis used in Claisen-Schmidt condensation. *Catalysts* **2022**, *12*, 759. [[CrossRef](#)]
41. Pavel, O.D.; Stamate, A.-E.; Zăvoianu, R.; Bucur, I.C.; Bîrjega, R.; Angelescu, E.; Pârvulescu, V.I. Mechano-chemical versus co-precipitation for the preparation of Y-modified LDHs for cyclohexene oxidation and Claisen-Schmidt condensations. *Appl. Catal. A Gen.* **2020**, *605*, 117797. [[CrossRef](#)]
42. Prévot, V.; Casala, B.; Ruiz-Hitzky, E. Intracrystalline alkylation of benzoate ions into layered double hydroxides. *J. Mater. Chem.* **2001**, *11*, 554–560. [[CrossRef](#)]
43. Mastalir, Á.; Király, Z. Pd nanoparticles in hydrotalcite: Mild and highly selective catalysts for alkyne semihydrogenation. *J. Catal.* **2003**, *220*, 372–381. [[CrossRef](#)]
44. Carja, G.; Delahay, G. Mesoporous mixed oxides derived from pillared oxovanadates layered double hydroxides as new catalysts for the selective catalytic reduction of NO by NH₃. *Appl. Catal. B Environ.* **2004**, *47*. [[CrossRef](#)]
45. Miyata, S. The Syntheses of Hydrotalcite-Like Compounds and Their Structures and Physico-Chemical Properties—I: The Systems Mg²⁺-Al³⁺-NO₃⁻, Mg²⁺-Al³⁺-Cl⁻, Mg²⁺-Al³⁺-ClO₄⁻, Ni²⁺-Al³⁺-Cl⁻ and Zn²⁺-Al³⁺-Cl⁻. *Clays Clay Miner.* **1975**, *23*, 369–375. [[CrossRef](#)]
46. Yousefi, S.; Ghasemi, B.; Tajally, M.; Asghari, A. Optical properties of MgO and Mg(OH)₂ nanostructures synthesized by a chemical precipitation method using impure brine. *J. Alloys Compd.* **2017**, *711*, 521–529. [[CrossRef](#)]
47. Sakamoto, K.; Ohno-Okumura, E. Syntheses and Functional Properties of Phthalocyanines. *Materials* **2009**, *2*, 1127–1179. [[CrossRef](#)]
48. Zhang, C.; Tong, S.W.; Jiang, C.; Kang, E.T.; Chan, D.S.H.; Zhu, C. Simple tandem organic photovoltaic cells for improved energy conversion efficiency. *Appl. Phys. Lett.* **2008**, *92*, 68. [[CrossRef](#)]
49. Rajendran, K.; Balakrishnan, G.S.; Kalirajan, J. Synthesis of Magnetite Nanoparticles for Arsenic Removal from Ground Water Pond. *Int. J. PharmTech Res.* **2015**, *8*, 670–677.
50. Pavel, O.D.; Zăvoianu, R.; Bîrjega, R.; Angelescu, E.; Pârvulescu, V.I. Mechanochemical versus co-precipitated synthesized lanthanum-doped layered materials for olefin oxidation. *Appl. Catal. A Gen.* **2017**, *542*, 10–20. [[CrossRef](#)]
51. Huang, F.; Tian, S.; Qi, Y.; Li, E.; Zhou, L.; Qiu, Y. Synthesis of FePcS-PMA-LDH Cointercalation Composite with Enhanced Visible Light Photo-Fenton Catalytic Activity for BPA Degradation at Circumneutral pH. *Materials* **2020**, *13*, 1951. [[CrossRef](#)]
52. Hur, T.-B.; Phuoc, T.X.; Chyu, M.K. New approach to the synthesis of layered double hydroxides and associated ultrathin nanosheets in de-ionized water by laser ablation. *J. Appl. Phys.* **2010**, *108*, 114312. [[CrossRef](#)]
53. Nairi, V.; Medda, L.; Monduzzi, M.; Salis, A. Adsorption and release of ampicillin antibiotic from ordered mesoporous silica. *J. Colloid Interface Sci.* **2017**, *497*, 217–225. [[CrossRef](#)] [[PubMed](#)]
54. Elhaci, A.; Labeled, F.; Khenifi, A.; Bouberka, Z.; Kameche, M.; Benabbou, K. MgAl-Layered double hydroxide for amoxicillin removal from aqueous media. *J. Environ. Anal. Chem.* **2020**, *101*, 2876–2898. [[CrossRef](#)]
55. Dogan, S.; Kidak, R. A Plug flow reactor model for UV-based oxidation of amoxicillin. *Desalin. Water Treat.* **2016**, *57*, 13586–13599. [[CrossRef](#)]